Nuclear Physics B415 (1994) 265–292
North-Holland

NUCLEAR PHYSICS B

Heavy quarks and leptons at e^+e^- colliders *

Alessandro Ballestrero
INFN, Sezione di Torino, I-10125 Turin, Italy

Ezio Maina
Dipartimento di Fisica Teorica, Università di Torino, and INFN, Sezione di Torino, I-10125 Turin, Italy

Stefano Moretti
INFN, Sezione di Torino, I-10125 Turin, Italy

Received 17 February 1993
(Revised 3 June 1993)
Accepted for publication 3 September 1993

The production of massive quarks and leptons in e^+e^- collisions is studied using exact helicity amplitudes. Total cross sections as a function of y_{cut}, in both the JADE and the k_T algorithms, are presented and compared with massless results. Some invariant-mass distributions are examined in relation to Higgs detection. Compact expressions for the helicity amplitudes are given.

1. Introduction

Massive particles are abundantly produced at e^+e^- colliders. Often they are associated with other, massless, particles in rather complicated final states. Whether masses are important or whether they can be ignored, depends on the center-of-mass energy and also on the region in phase space which is under study. For instance, the electron mass can be ignored in most cases at LEP energies, but for its role in regulating collinear divergences in reactions like Bhabha scattering at small angles. On the contrary, the top mass is so large that it must be included in all cases even at supercollider energies. In a recent paper [1] we have shown that at the Z^0 peak, when masses are properly taken into account, cross sections involving b or, to a lesser extent, c quarks differ significantly from the corresponding predictions obtained when masses are neglected. It is the purpose of this paper to

* Work supported in part by Ministero dell'Università e della Ricerca Scientifica.

SSDI 0550-3213(93)E0461-8

extend these results in several directions. To this end we compute and present the helicity amplitudes for a number of e^+e^- processes with three and four particles in the final state in which masses can be relevant. We make no approximation and consider all contributions due to intermediate γ's and Z^0's. Therefore our matrix elements are exact at any energy and we consider both LEP I and LEP II. At higher center-of-mass energy, mass effects are expected to be smaller, but only an explicit calculation can establish to which degree this is correct. On the other hand, one of the main task of LEP II will be to search for the Higgs boson in the mass range 45 GeV $\leqslant m_H \leqslant$ 80 GeV [2]. Such a Higgs decays almost exclusively to $b\bar{b}$ and $\tau^+\tau^-$ and as a consequence it is important to determine as accurately as possible all reactions in which $b\bar{b}$ and $\tau^+\tau^-$ pairs are produced, which could provide a background to Higgs detection.

Studying the production of up to four strongly interacting particles, we examine jet–jet mass distributions, the effects of different clustering algorithms, and the relevance of mass effects for shape variables. Four-quark final states with quarks of different flavors are also examined, as well as the production of two quarks and two leptons and of four leptons. These kind of events are relevant as a potential background to Higgs searches and provide a test of the Standard Model, though not at the level of precision which can be reached in more inclusive measurements. Finally we consider final states including photons which are actively studied experimentally in order to determine the electroweak couplings of the quarks, and as a mean to search for new phenomena.

The calculation of multi-jet production in e^+e^- reactions has a long history [3–16], dating back to the times when jets were first observed in e^+e^- collisions at PEP and PETRA. At those energies the Z^0 contribution was small and could be safely ignored [3–7,9,11]. Masses were already taken into account for these processes. Apart from the simplest cases [3,4], only the cross sections for massless fermions were compact enough to be published [5,7,10]. With the advent of LEP and the advances in spinor techniques * these results were improved in various ways. In particular in ref. [13] the complete triply differential cross section for $e^+e^- \to Q\bar{Q}g$ for massive quarks with both an intermediate photon and Z^0 was presented. In ref. [14] the decay $Z \to 4f$ was studied. From their expression it is possible to reconstruct the full amplitude for $e^+e^- \to 4f$. Recently, very simple formulae for $e^+e^- \to q\bar{q}gg$, $q\bar{q}q\bar{q}$ have been given [15] for massless quarks.

Using the Z-function formalism [11,18], which is based on the results of ref. [19], we are able to give particularly compact expressions, valid for both massive and massless fermions, in which it is easy to substitute one vector boson with a different one in any part of a diagram. The helicity amplitudes for $e^+e^- \to f\bar{f}V$, with $V = \gamma, g, Z^0$, $e^+e^- \to f\bar{f}gg$, $e^+e^- \to f\bar{f}\gamma g$ including initial state radiation and $e^+e^- \to f\bar{f}f'\bar{f}'$ with $f \neq e$ are presented in Appendix B.

* For a good introduction to helicity methods and complete references, see ref. [17].

The matrix element for all processes for which we give results has also been computed following the method of ref. [20] as a check of the correctness of our results.

In Appendix A, for the convenience of the reader, we briefly recall the method and the results of refs. [18,19] and we collect various formulae which are used in the analytic expressions.

The amplitudes have been checked for gauge invariance, and for BRST invariance [21] in case of external Z^0's. In the appropriate limits our results reproduce those of refs. [3,11,15] after some misprints in the formulae of ref. [15] have been corrected.

We have used $M_Z = 91.1$ GeV, $\Gamma_Z = 2.5$ GeV, $\sin^2\theta_W = 0.23$, $\alpha_s = 0.115$, $\alpha_{em} = \frac{1}{128}$, $m_\tau = 1.78$ GeV, $m_c = 1.7$ GeV and $m_b = 5.0$ GeV in the numerical part of our work.

In what follows we neglect all hadronization effects, and apply cuts at the partonic level.

2. Jets

All LEP experiments have performed a large number of QCD tests. For instance, mentioning only the measurements which are most likely to be sensitive to masses, α_s has been determined from jet rates and shape variables [22]. Flavor independence of the coupling has been verified [23]. Three- [24] and four- [25] jet distributions have been studied and compared with QCD predictions. The color factors, which determine the gauge group which is responsible for strong interactions, have been measured [26]. The possibility of tagging quark jets using the semileptonic decays of b and c quarks has been exploited, for example in studies of the differences between gluon and quark jets [27].

In the coming years, improvements in statistics, in secondary vertex reconstruction with silicon vertex detectors and in particle identification will allow much more detailed studies of heavy-quark production at LEP.

The experimental definition of a jet is based on a clustering procedure. The two most widely used schemes are the JADE algorithm [28] based on the variable

$$y_{ij}^{J} = 2\frac{E_i E_j}{E_{vis}^2}(1 - \cos\theta_{ij}) \tag{1}$$

and the k_T or Durham algorithm [29] which makes use of a new clustering variable

$$y_{ij}^{T} = 2\frac{\min(E_i^2, E_j^2)}{E_{vis}^2}(1 - \cos\theta_{ij}). \tag{2}$$

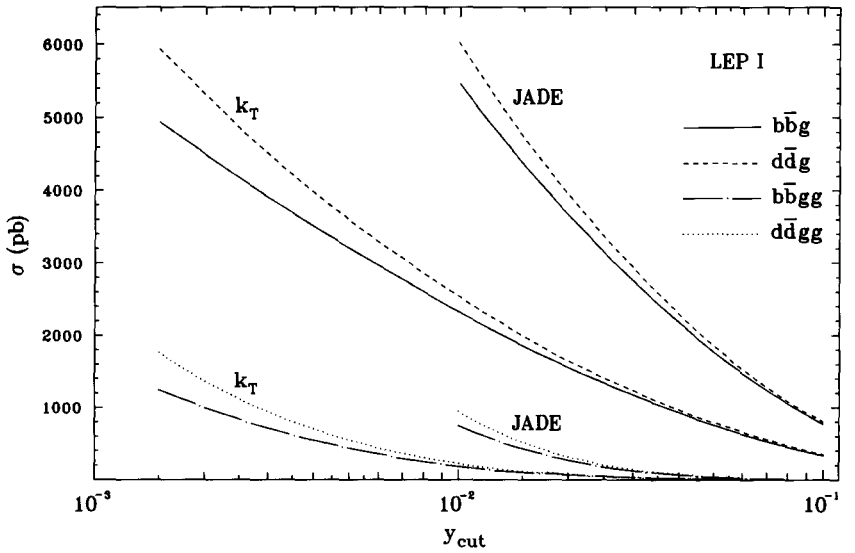

Fig. 1. Cross sections for $e^+e^- \to b\bar{b}g$ (continuous), $e^+e^- \to d\bar{d}g$ (dashed), $e^+e^- \to b\bar{b}gg$ (chain-dotted) and $e^+e^- \to d\bar{d}gg$ (dotted) as a function of y_{cut} for both definitions of y at $\sqrt{s} = 91.1$ GeV.

In fig. 1 we present the cross sections for $e^+e^- \to q\bar{q}g$ and $e^+e^- \to q\bar{q}gg$ with q = d, b as a function of y_{cut} for both definitions of y at LEP I. For small y_{cut}^T the cross section for $b\bar{b}g$ is almost 20% smaller than for $d\bar{d}g$. As expected the ratio becomes closer to one for larger y_{cut}, but for y_{cut} as large as 0.2 still $R_3^{bd} = \sigma(b\bar{b}g)/\sigma(d\bar{d}g) \leqslant 0.96$ in both schemes. The cross sections for the same reactions at $\sqrt{s} = 200$ GeV are given in fig. 2. The differences between the massive and the massless case are less important at higher energies, as expected, but still of the order of several percent. It has to be noticed that the Durham scheme tends to enhance these differences. This feature has been found in all cross sections and distributions we have studied. Therefore, depending on the kind of analysis which is performed on the data sample, different schemes can be used in order to exalt or suppress mass effects. A typical example of this behavior is shown in figs. 3a and 3b where the invariant-mass distributions in three-jet events are presented. The different shape of b and d events is quite noticeable for the Durham algorithm, not only for the invariant mass of the qg pair, which is expected because of the different quark-energy threshold, but also for the invariant mass of the $q\bar{q}$ pair. The exact shape of these distributions depends on y_{cut} but the different sensitivity to mass effects in the two schemes remains.

The $q\bar{q}gg$ final state is the dominant contribution to the four-jet cross section. The process with two hard-gluon emissions is more sensitive to masses than the process with only one emission. For instance $R_4^{bd} = \sigma(b\bar{b}gg)/\sigma(d\bar{d}gg) = 0.7$ for $y_{cut}^T = 1.5 \times 10^{-3}$.

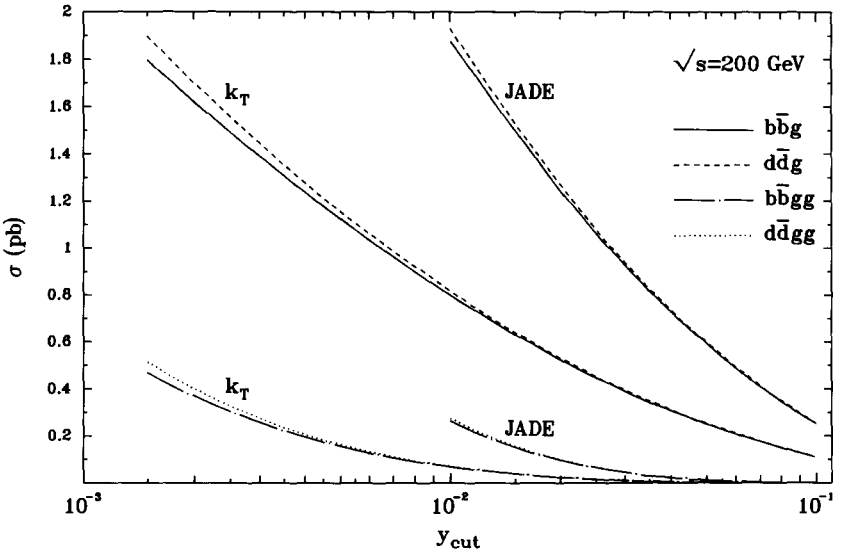

Fig. 2. Cross sections for $e^+e^- \to b\bar{b}g$ (continuous), $e^+e^- \to d\bar{d}g$ (dashed), $e^+e^- \to b\bar{b}gg$ (chain-dotted) and $e^+e^- \to d\bar{d}gg$ (dotted) as a function of y_{cut} for both definitions of y at $\sqrt{s} = 200$ GeV.

The various contributions to $e^+e^- \to q\bar{q}q'\bar{q}'$ are shown in fig. 4 ($q = q'$) and fig. 5 ($q \neq q'$) as a function of y_{cut}. Though very small compared with the $q\bar{q}gg$ rates these cross sections could be quite interesting if heavy quarks can be tagged with high efficiency. For 10^6 Z^0, corresponding to an integrated luminosity of about 30 pb^{-1}, one expects approximately 100 events with four b quarks and 400 events with two b and two c quarks at $y^J_{cut} = 1.0 \times 10^{-2}$. The differences between massive and massless results are large, and even the charm mass has a significant effect. It is interesting to notice that the cross section for $b\bar{b}u\bar{u}$ is larger than the cross section for $b\bar{b}d\bar{d}$, contrary to the naive expectations based on the fact that down-type quarks couple more strongly to the Z^0 than up-type quarks. This is due to the interference between graphs 1 and 2 with graphs 3 and 4 of fig. B.1a.

From figs. 1, 2, 4 and 5 it can be seen that, while for three-parton processes the cross sections for $y^J_{cut} = 1.0 \times 10^{-2}$ are approximately matched by the cross sections for $y^T_{cut} = 1.5 \times 10^{-3}$, in the four-parton case this happens for $y^T_{cut} = 3.0 \times 10^{-3}$.

Jet-shape variables have been extensively studied as a tool to determine α_s and as a testing ground for the agreement between data and the standard description of strong interactions. The value of α_s is extracted for each variable, comparing, in a suitable range, the analytical $O(\alpha_s^2)$ expression [30] with the data, corrected for hadronization and detector effects. In the ranges used for measuring α_s, the ratio of massive to massless tree-level predictions can differ significantly from unity and it depends both on the variable and on its actual value. We have compared at

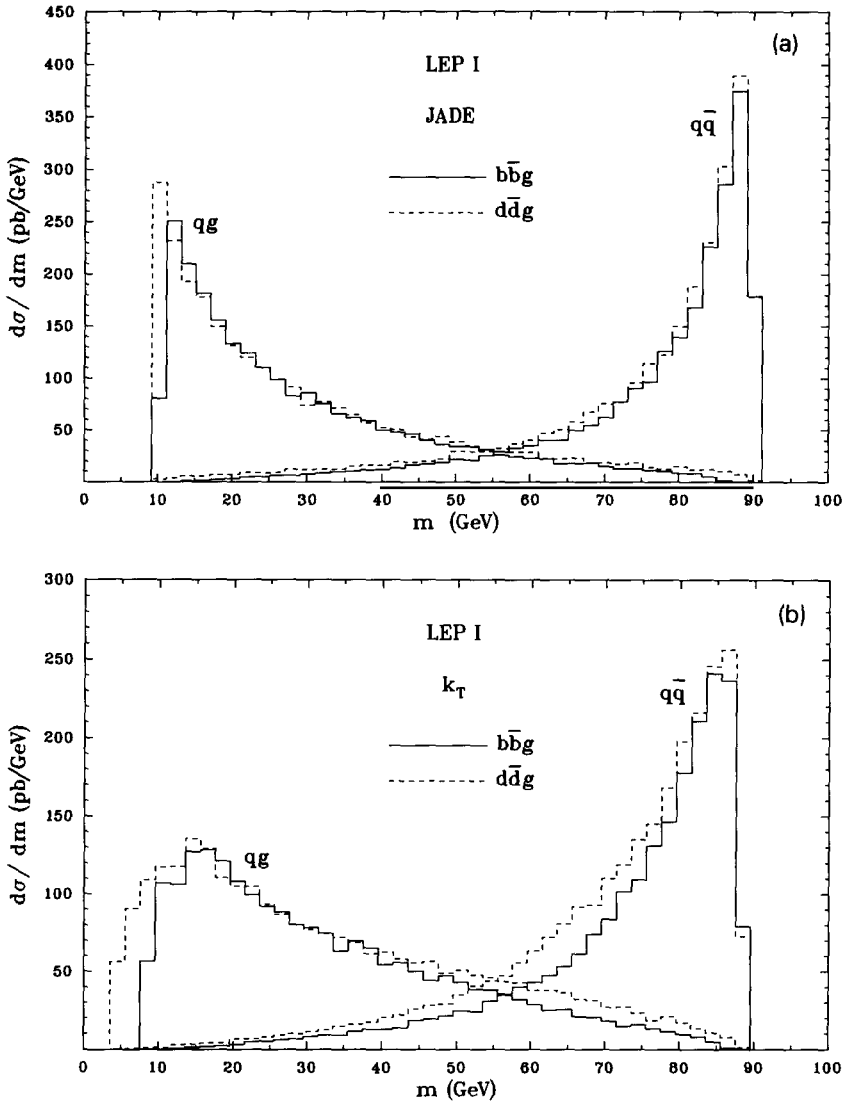

Fig. 3. Mass distributions for the qg pair and for the $q\bar{q}$ pair in $e^+e^- \to b\bar{b}g$ (continuous) and $e^+e^- \to d\bar{d}g$ (dashed) events in (a) the JADE and (b) k_T schemes at $\sqrt{s} = 91.1$ GeV. All particle pairs have (a) $y_{ij}^J \geqslant 1.0 \times 10^{-2}$, (b) $y_{ij}^T \geqslant 1.5 \times 10^{-3}$.

$O(\alpha_s)$ the ratio $R_{\gamma Z}$, which is obtained from the full matrix element, with R_γ the ratio which results neglecting the Z^0, for thrust, oblateness, C-parameter, M_H and M_D. Up to now in fact, mass effects for shape variables have normally been evaluated using JETSET [37] from which only R_γ can be extracted. $R_{\gamma Z}$ is consistently smaller than R_γ. This is obviously related to the larger influence of

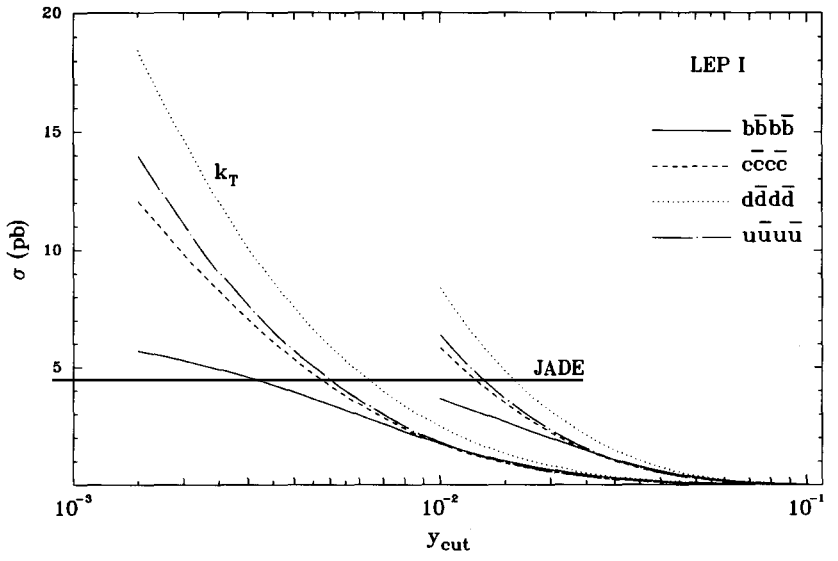

Fig. 4. Cross sections for $e^+e^- \to q\bar{q}q\bar{q}$, q = d (dotted), u (chain-dotted), c (dashed) and b (continuous) as a function of y_{cut} for both definitions of y at $\sqrt{s} = 91.1$ GeV.

mass effects on the axial part of the amplitude compared to the vector part. The difference turns out to be about 1.2×10^{-2}, almost independent of the particular variable and of its specific value. As an example, in fig. 6 we show both $R_{\gamma Z}$ and

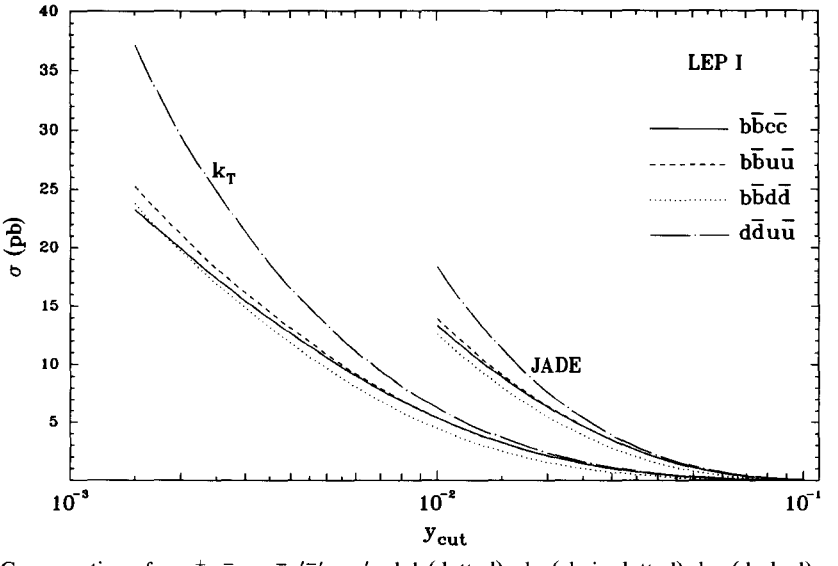

Fig. 5. Cross sections for $e^+e^- \to q\bar{q}q'\bar{q}'$, $qq' = bd$ (dotted), du (chain-dotted), bu (dashed) and bc (continuous) as a function of y_{cut} for both definitions of y at $\sqrt{s} = 91.1$ GeV.

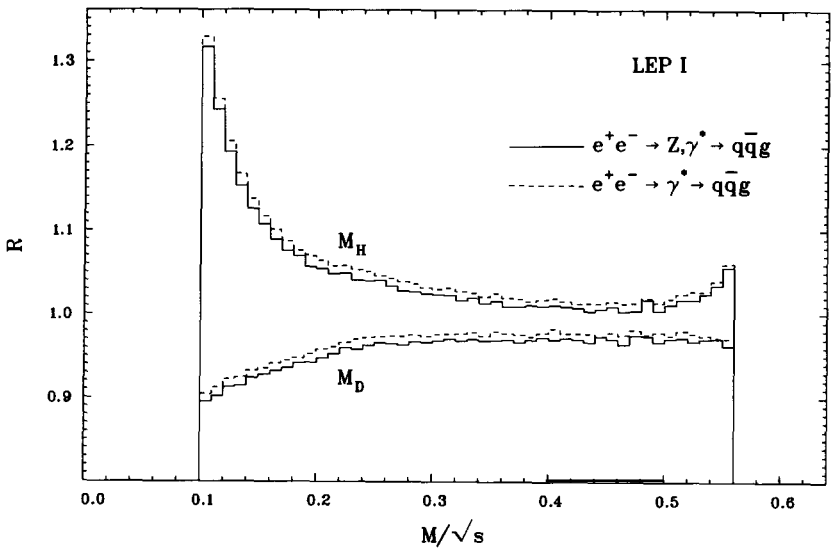

Fig. 6. The ratio $R = d\sigma(b\bar{b}g)/d\hat{M}/d\sigma(d\bar{d}g)/d\hat{M}$ for $\hat{M} = M_H/\sqrt{s}$ and $\hat{M} = M_D/\sqrt{s}$ from the full matrix element (continuous) and from the photon contribution alone (dashed) at $\sqrt{s} = 91.1$ GeV.

R_γ for the M_H and M_D distributions. Our results show that the complete mass corrections can be obtained with a simple additional factor. A further comment is in order. The theoretical three-jet rate is a combination of three- and four-parton processes, the four-parton contribution being of the order of 20% in the Durham scheme at small y_{cut}. From our figures it is clear that the mass-correction factors for three- and four-parton reactions differ considerably and therefore the simple method adopted in order to evaluate mass corrections, based exclusively on three-parton processes, might slightly underestimate them.

3. Backgrounds to Higgs searches

The main production mechanism [2] for the Higgs particle at LEP II energies is $e^+e^- \to HZ$. If the Higgs mass is between 40 and 80 GeV the cross section for this process is of the order of 1 pb. Four-jet events are a potential source of background to $e^+e^- \to HZ \to b\bar{b}jj$. If b's can be efficiently tagged, the main background contribution is given by $e^+e^- \to b\bar{b}gg$. For this reason we have computed the invariant-mass distributions of all particle pairs in the $b\bar{b}gg$ final state. The distributions is shown in fig. 7 at $\sqrt{s} = 200$ GeV. We have required $y_{ij}^T \geqslant 1.5 \times 10^{-3}$ for all pairs and that the angle of each particle with the beam satisfies $|\cos\theta| < 0.95$. The $b\bar{b}$ mass peaks well above 100 GeV while the gg mass clusters at small invariant masses. The cross section for 40 GeV $\leqslant m_{b\bar{b}} \leqslant 80$ GeV is only about 5×10^{-2} pb, which corresponds to approximately 25 events. Moreover, since

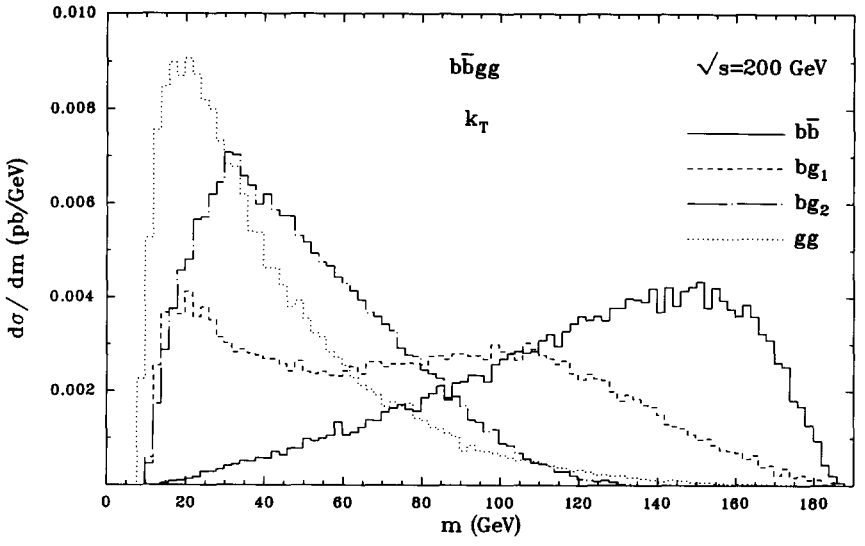

Fig. 7. Two-jet invariant-mass distributions in $e^+e^- \to b\bar{b}gg$ at $\sqrt{s} = 200$ GeV. The pairs are $b\bar{b}$ (continuous), bg_1 (dashed), bg_2 (chain-dotted) and gg (dotted), where g_1 (g_2) is the most (least) energetic of the two gluons. All particle pairs have $y_{ij}^{T} \geqslant 1.5 \times 10^{-3}$. The angle of each particle with the beam satisfies $|\cos\theta| < 0.95$.

the two gluons should fake a hadronic decay of the Z^0, one could impose a cut on their invariant mass, decreasing this background drastically. The distribution at $\sqrt{s} = 170$ GeV, a realistic energy for the first phase of LEP II, is similar but about two times larger.

The Higgs-production cross section times the branching ratio to $\tau^+\tau^-$ at LEP II energies is about 80 fb. Hence it might be possible to detect the Higgs in this channel and to measure its coupling to the τ. A comparison of this decay mode with the dominant one to $b\bar{b}$ would test the predicted proportionality of Higgs coupling to fermion masses. We have computed $\tau^+\tau^-$ pair production in $e^+e^- \to \tau^+\tau^- q\bar{q}$ at $\sqrt{s} = 170$ GeV summed over five massless flavors. In order to select events which could fake a hadronic decay of the Z^0 we have required the invariant mass of the $q\bar{q}$ pair to be larger than 60 GeV. The cross section integrated for the $\tau^+\tau^-$ invariant mass between 40 and 70 GeV is less than 10 fb. Hence this background is rather small. On the other hand, with the mentioned cut, $\sigma(e^+e^- \to \tau^+\tau^- q\bar{q}) = 86$ fb. This result is comparable to the Higgs-production cross section in the $\tau^+\tau^-$ channel and it can be used as a reference point for the Higgs search.

4. Jets plus leptons and four leptons

Four-fermion final states with at least one lepton pair are relatively easy to study experimentally, and in some cases they represent a potential background to

TABLE 1
Total cross sections for $e^+e^- \to \tau^+\tau^-\tau^+\tau^-$, $e^+e^- \to \tau^+\tau^- c\bar{c}$ and $e^+e^- \to \tau^+\tau^- b\bar{b}$ at $\sqrt{s} = 91.1$ and 200 GeV. Errors are as given by VEGAS [34]

Channel	σ_{tot} (10^{-4} pb)	
	LEP I ($\sqrt{s} = 91.1$ GeV)	LEP II ($\sqrt{s} = 200$ GeV)
$\tau^+\tau^-\tau^+\tau^-$	876.4 ± 4.3	57.8 ± 2.0
$\tau^+\tau^- c\bar{c}$	2266.7 ± 8.0	269.5 ± 3.5
$\tau^+\tau^- b\bar{b}$	406.2 ± 1.7	289.9 ± 4.7

Higgs production. Much interest has been spurred by the observation of an apparent excess in the $\tau^+\tau^-X$ channel in ALEPH's 1989–1990 data [31]. This observation has not been confirmed by other collaborations [32].

Quite recently a new Monte Carlo [33], which includes fermion masses and a complete treatment of γ and Z^0 contributions as is appropriate outside the Z^0 peak, and which combines them with initial- and final-state radiation and with a careful mapping of the many peaks in the matrix element due to collinear configurations, has been presented. We have computed the cross section for $e^+e^- \to \mu^+\mu^-\tau^+\tau^-$ and $e^+e^- \to \tau^+\tau^-\tau^+\tau^-$, without initial-state radiation, with the parameters used in ref. [33] and we obtain $\sigma_{tot}(e^+e^- \to \mu^+\mu^-\tau^+\tau^-) = 640.0 \pm 7.0$ fb and $\sigma_{tot}(e^+e^- \to \tau^+\tau^-\tau^+\tau^-) = 61.2 \pm 0.3$ fb, in excellent agreement with that reference.

In table 1 we give the total cross sections for $e^+e^- \to \tau^+\tau^-\tau^+\tau^-$, $e^+e^- \to \tau^+\tau^- c\bar{c}$ and $e^+e^- \to \tau^+\tau^- b\bar{b}$ at $\sqrt{s} = 91.1$ and 200 GeV with the standard parameters used in this paper, in particular with $\alpha_{em} = \frac{1}{128}$ at all electroweak vertices. The expected number of events is very small, between one and five events per 10^6 Z^0 at LEP I.

5. Final states including a photon or Z^0

Photons are the only particles which can be directly revealed and couple to the quarks in the early stages of the hadronization process. Final-state radiation in multihadronic decays of the Z^0 can be used to test the electroweak couplings of up- and down-type quarks [35,36], combining the measurement of the radiation rate with the measured hadronic width of the Z^0.

In fig. 8 we give the cross sections for $e^+e^- \to q\bar{q}\gamma$ and $e^+e^- \to q\bar{q}\gamma g$, with $q = d, b$, at the Z^0 peak as a function of y_{cut}. The photon transverse momentum is required to be greater than 5 GeV. The difference between b and d quarks is again quite important both for $\sigma(y_{cut})$ and for the photon-energy spectrum which is given in fig. 9.

In table 2 we present the total cross section for production of a Z^0 in association with a heavy-fermion pair at $\sqrt{s} = 200$ GeV. We implicitly assume that

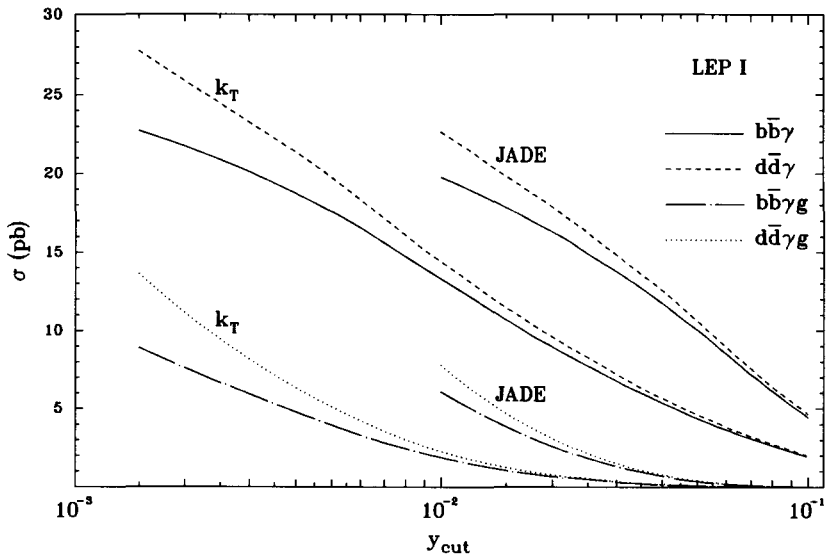

Fig. 8. Cross sections for $e^+e^- \to b\bar{b}\gamma$ (continuous), $e^+e^- \to d\bar{d}\gamma$ (dashed), $e^+e^- \to b\bar{b}\gamma g$ (chain-dotted) and $e^+e^- \to d\bar{d}\gamma g$ (dotted) as a function of y_{cut} at $\sqrt{s} = 91.1$ GeV. All particle pairs have $y > y_{cut}$. The photon transverse momentum is required to be greater than 5 GeV.

the Z^0 decays to a fermion pair different from the one that appears in the event. These processes are dominated by the diagrams in fig. B.2b. Our results show that both the intermediate photon and Z^0 give a sizable contribution. In fact if only

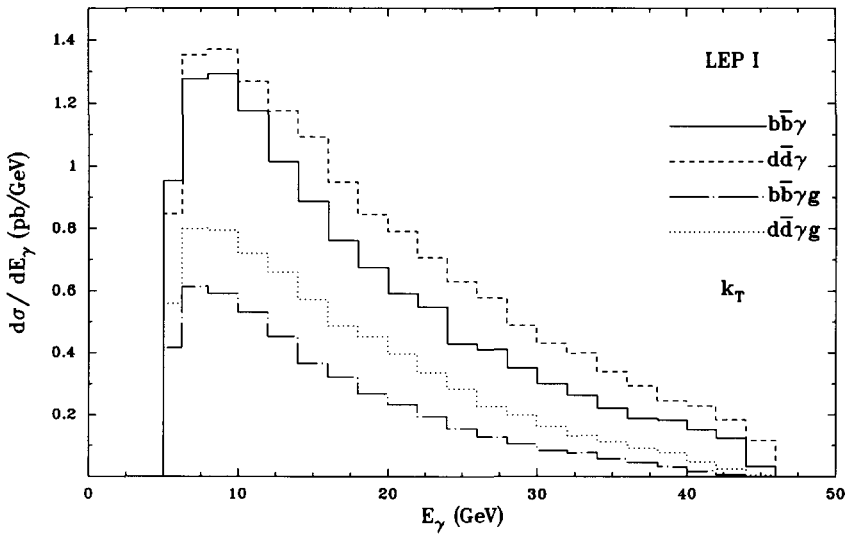

Fig. 9. Photon-energy spectra in $e^+e^- \to b\bar{b}\gamma$ (continuous), $e^+e^- \to d\bar{d}\gamma$ (dashed), $e^+e^- \to b\bar{b}\gamma g$ (chain-dotted) and $e^+e^- \to d\bar{d}\gamma g$ (dotted) at $\sqrt{s} = 91.1$ GeV. All particle pairs have $y_{ij}^T \geq 1.5 \times 10^{-3}$. The photon transverse momentum is required to be greater than 5 GeV.

TABLE 2
Total cross sections for $e^+e^- \to Z\mu^+\mu^-$, $e^+e^- \to Z\tau^+\tau^-$, $e^+e^- \to Zc\bar{c}$ and $e^+e^- \to Zb\bar{b}$ at $\sqrt{s} = 200$ GeV. Errors are as given by VEGAS [34]

Channel	σ_{tot} (10^{-3} pb) LEP II ($\sqrt{s} = 200$ GeV)
$Z^0\mu^+\mu^-$	341.1 ±1.9
$Z^0\tau^+\tau^-$	170.01 ±0.64
$Z^0c\bar{c}$	402.4 ±1.0
$Z^0b\bar{b}$	378.19 ±0.71

diagrams with two Z^0's were important one would expect $\sigma(e^+e^- \to Z\mu^+\mu^-) \approx \sigma(e^+e^- \to Z\tau^+\tau^-)$; if, on the contrary, only photonic intermediate states were relevant one would get $\sigma(e^+e^- \to Zc\bar{c}) \approx 3 \times (\frac{2}{3})^2 \sigma(e^+e^- \to Z\tau^+\tau^-)$. All processes produce rates of the order of 100 events for 500 pb^{-1} of integrated luminosity.

6. Conclusions

We have computed the exact matrix elements, at tree level, for a number of processes at e^+e^- colliders with three and four particles in the final state in which masses are relevant. We have given the corresponding helicity amplitudes in the Z-function formalism. We have studied these processes at LEP I and LEP II energies using both the JADE and the Durham clustering algorithm.

Total cross sections involving b quarks are substantially smaller than the corresponding ones for d quarks, particularly for small y_{cut}. The effect increases with the number of jets and (obviously) with the number of massive particles. The differences between the cross sections or distributions for massive quarks and those with massless ones are generally larger in the Durham algorithm. Mass effects on shape variables have been studied.

Four-jet events involving heavy particles and two-tau-two-jet events are a possible background to Higgs production. We have computed their rates, which, in the relevant mass regions, are much smaller than Higgs production.

We have presented cross sections and energy distributions for one-photon production in association with up to three jets, keeping quark masses into account.

Appendix A

THE HELICITY AMPLITUDE METHOD

In this section, for completeness, we briefly recall the spinor techniques of refs. [18,19] which are used in our calculations.

A.1. SPINORS

External fermions * of mass m and momentum p^μ are described by spinors corresponding to states of definite helicity λ, $u(p, \lambda)$ verifying the Dirac equations

$$\not{p}u(p, \lambda) = \pm m u(p, \lambda),$$

$$\bar{u}(p, \lambda)\not{p} = \pm m\bar{u}(p, \lambda) \tag{A.1}$$

and the spin-sum relation

$$\sum_{\lambda = \pm} u(p, \lambda)\bar{u}(p, \lambda) = \not{p} \pm m, \tag{A.2}$$

where the sign + (−) refers to a particle (antiparticle).

One can choose two arbitrary vectors k_0 and k_1 such that

$$k_0 \cdot k_0 = 0, \quad k_1 \cdot k_1 = -1, \quad k_0 \cdot k_1 = 0, \tag{A.3}$$

and express the spinors $u(p, \lambda)$ in terms of chiral ones $w(k_0, \lambda)$ as

$$u(p, \lambda) = w(p, \lambda) + \mu w(k_0, -\lambda), \tag{A.4}$$

where

$$w(p, \lambda) = \not{p} w(k_0, -\lambda)/\eta \tag{A.5}$$

and

$$\mu = \pm m/\eta, \quad \eta = \sqrt{2(p \cdot k_0)}\,. \tag{A.6}$$

The spinors $w(k_0, \lambda)$ satisfy

$$w(k_0, \lambda)\bar{w}(k_0, \lambda) = \tfrac{1}{2}(1 + \lambda\gamma_5)\not{k}_0 \tag{A.7}$$

and therefore

$$\sum_{\lambda = \pm} w(k_0, \lambda)\bar{w}(k_0, \lambda) = \not{k}_0. \tag{A.8}$$

The phase between chiral states is fixed by

$$w(k_0, \lambda) = \lambda \not{k}_1 w(k_0, -\lambda). \tag{A.9}$$

The freedom in choosing k_0 and k_1 provides a powerful tool for checking the correctness of any calculation.

* Unless stated otherwise, we shall use the term "fermion" and the symbol u for both particles and antiparticles.

A.2. POLARIZATION VECTORS FOR MASSLESS GAUGE BOSONS

External spin-1 massless gauge bosons of momentum p^μ are described by polarization vectors corresponding to states of definite helicity λ, $\epsilon^\mu(p, \lambda)$ satisfying

$$\epsilon(p, \lambda)\cdot p = 0, \quad \epsilon(p, \lambda)\cdot\epsilon(p, \lambda) = 0,$$

$$\epsilon^\mu(p, -\lambda) = \epsilon^{\mu *}(p, \lambda), \quad \epsilon(p, \lambda)\cdot\epsilon(p, -\lambda) = -1 \tag{A.10}$$

and the spin-sum relation (in the axial gauge)

$$\sum_{\lambda=\pm} \epsilon^\mu(p, \lambda)\epsilon^{\nu *}(p, \lambda) = -g^{\mu\nu} + \frac{q^\mu p^\nu + q^\nu p^\mu}{p\cdot q}, \tag{A.11}$$

where q^μ is any four-vector not proportional to p^μ.

Any object $\epsilon^\mu(p, \lambda)$ obeying the relations (A.10), (A.11) makes an acceptable choice for the polarization vectors. For instance

$$\epsilon^\mu(p, \lambda) = N[\bar{u}(p, \lambda)\gamma^\mu u(q, \lambda)], \tag{A.12}$$

N being the normalization factor

$$N = [4(q\cdot p)]^{-1/2}. \tag{A.13}$$

The existing freedom in choosing q^μ corresponds to fixing the gauge. The final results do not depend on the choice of q^μ.

A.3. POLARIZATION VECTORS FOR MASSIVE GAUGE BOSONS

For spin-1 massive gauge bosons there is an additional longitudinally polarized state satisfying

$$\epsilon(p, 0)\cdot p = 0, \quad \epsilon(p, \lambda)\cdot\epsilon(p, 0) = 0, \quad \epsilon(p, 0)\cdot\epsilon(p, 0) = -1. \tag{A.14}$$

The spin sum becomes

$$\sum_{\lambda=\pm,0} \epsilon^\mu(p, \lambda)\epsilon^{\nu *}(p, \lambda) = -g^{\mu\nu} + \frac{p^\mu p^\nu}{m^2}, \tag{A.15}$$

where m and p^μ are the gauge-boson mass and momentum, respectively.

For the polarization vectors of massive gauge bosons we cannot adopt the form (A.12), since for a timelike momentum p^μ we cannot assign a definite helicity in a covariant way to the spinors $u(p)$ and antispinors $v(p)$.

The simplest solution lies in noting that we are usually dealing with cross sections for unpolarized bosons, so we really have as the only requirement on the $\epsilon^\mu(p, \lambda)$ that their spin sum should be as in eq. (A.15). Any way by which we arrive at that expression gives us an acceptable choice for the polarization representation.

Introducing the quantity

$$a^\mu = \bar{u}(r_2, -)\gamma^\mu u(r_1, -), \tag{A.16}$$

where r_1^μ, r_2^μ are two lightlike four-vectors satisfying

$$r_1^2 = r_2^2 = 0, \quad r_1^\mu + r_2^\mu = p^\mu, \tag{A.17}$$

this can be used, after proper normalization, as the polarization vector belonging to p^μ. In fact, if we replace the spin sum by an integral over the solid angle $d\Omega$ of r_1 in the rest frame of p^μ, the result is of the desired form

$$\int d\Omega\, a^\mu a^{\nu *} = \tfrac{8}{3}\pi m^2 \left(-g^{\mu\nu} + \frac{p^\mu p^\nu}{m^2} \right). \tag{A.18}$$

This implies that we will obtain the correct result for the cross sections if we make the following replacements for on-shell massive bosons:

$$\epsilon^\mu \to a^\mu, \quad \sum \epsilon^\mu \epsilon^{\nu *} \to \frac{3}{8\pi m^2} \int d\Omega\, a^\mu a^{\nu *}. \tag{A.19}$$

A.4. *S* AND *Z* FUNCTIONS

Using the previous definitions one can compute

$$S(\lambda, p_1, p_2) = \bar{u}(p_1, \lambda) u(p_2, -\lambda) \tag{A.20}$$

and

$$\begin{aligned} &Z(p_1, \lambda_1; p_2, \lambda_2; p_3, \lambda_3; p_4, \lambda_4; c_R, c_L; c'_R, c'_L) \\ &\quad = \left[\bar{u}(p_1, \lambda_1) \Gamma^\mu u(p_2, \lambda_2) \right] \left[\bar{u}(p_3, \lambda_3) \Gamma'_\mu u(p_4, \lambda_4) \right], \end{aligned} \tag{A.21}$$

where

$$\Gamma^{(\prime)\mu} = \gamma^\mu \Gamma^{(\prime)} \tag{A.22}$$

and

$$\Gamma^{(\prime)} = \left(c_R^{(\prime)} P_R + c_L^{(\prime)} P_L \right), \tag{A.23}$$

with

$$P_R = \tfrac{1}{2}(1 + \gamma_5), \quad P_L = \tfrac{1}{2}(1 - \gamma_5), \tag{A.24}$$

the chiral projectors.

The results ($\epsilon^{0123} = 1$) are (see (A.6))

$$S(+, p_1, p_2) = 2\frac{(p_1\cdot k_0)(p_2\cdot k_1) - (p_1\cdot k_1)(p_2\cdot k_0) + i\epsilon_{\mu\nu\rho\sigma}k_0^\mu k_1^\nu p_1^\rho p_2^\sigma}{\eta_1\eta_2}, \quad \text{(A.25)}$$

$$S(-, p_1, p_2) = S(+, p_2, p_1)^* \quad \text{(A.26)}$$

and

$$\begin{aligned}
&Z(p_1, +; p_2, +; p_3, +; p_4, +; c_R, c_L; c'_R, c'_L)\\
&\quad = -2[S(+, p_3, p_1)S(-, p_4, p_2)c'_R c_R - \mu_1\mu_2\eta_3\eta_4 c'_R c_L - \eta_1\eta_2\mu_3\mu_4 c'_L c_R],\\
&Z(p_1, +; p_2, +; p_3, +; p_4, -; c_R, c_L; c'_R, c'_L)\\
&\quad = -2\eta_2 c_R[S(+, p_4, p_1)\mu_3 c'_L - S(+, p_3, p_1)\mu_4 c'_R],\\
&Z(p_1, +; p_2, +; p_3, -; p_4, +; c_R, c_L; c'_R, c'_L)\\
&\quad = -2\eta_1 c_R[S(-, p_2, p_3)\mu_4 c'_L - S(-, p_2, p_4)\mu_3 c'_R],\\
&Z(p_1, +; p_2, +; p_3, -; p_4, -; c_R, c_L; c'_R, c'_L)\\
&\quad = -2[S(+, p_1, p_4)S(-, p_2, p_3)c'_L c_R - \mu_1\mu_2\eta_3\eta_4 c'_L c_L - \eta_1\eta_2\mu_3\mu_4 c'_R c_R],\\
&Z(p_1, +; p_2, -; p_3, +; p_4, +; c_R, c_L; c'_R, c'_L)\\
&\quad = -2\eta_4 c'_R[S(+, p_3, p_1)\mu_2 c_R - S(+, p_3, p_2)\mu_1 c_L],\\
&Z(p_1, +; p_2, -; p_3, +; p_4, -; c_R, c_L; c'_R, c'_L) = 0,\\
&Z(p_1, +; p_2, -; p_3, -; p_4, +; c_R, c_L; c'_R, c'_L)\\
&\quad = -2[\mu_1\mu_4\eta_2\eta_3 c'_L c_L + \mu_2\mu_3\eta_1\eta_4 c'_R c_R - \mu_2\mu_4\eta_1\eta_3 c'_L c_R - \mu_1\mu_3\eta_2\eta_4 c'_R c_L],\\
&Z(p_1, +; p_2, -; p_3, -; p_4, -; c_R, c_L; c'_R, c'_L)\\
&\quad = -2\eta_3 c'_L[S(+, p_2, p_4)\mu_1 c_L - S(+, p_1, p_4)\mu_2 c_R].
\end{aligned} \quad \text{(A.27)}$$

The remaining Z functions can be obtained by exchanging $+ \leftrightarrow -$ and $R \leftrightarrow L$.

Appendix B

MATRIX ELEMENTS

In this section we give the analytic formulae for the matrix elements. We define the propagator functions as

$$D_{\gamma,g}(p) = \frac{1}{p^2}, \quad D_Z(p) = \frac{1}{\sin^2\theta_W \cos^2\theta_W (p^2 - M_Z^2 + iM_Z\Gamma_Z)} \quad \text{(B.1)}$$

and

$$D_f(p) = \frac{1}{p^2 - m_f^2}, \tag{B.2}$$

where M_Z and Γ_Z are, respectively, the mass and the width of the Z boson, θ_W is the weak mixing angle and m_f is the fermion mass.

We also define

$$N_i = [4(q_i \cdot p_i)]^{-1/2}, \tag{B.3}$$

where p_i and q_i are the momentum and the auxiliary momentum of the ith massless vector boson, respectively.

Adopting for the polarization vectors of the gauge bosons the choices (A.12) and (A.16), and replacing any $\not{p}$ in the fermion propagator numerator with

$$\not{p} = \sum_{\lambda = \pm} u(p, \lambda)\bar{u}(p, \lambda) \mp m, \tag{B.4}$$

one can express the Feynman amplitude T for a generic diagram as

$$T = \alpha CDM, \tag{B.5}$$

where α indicates the couplings, D the appropriate combination of boson and/or fermion propagators functions, C the eventual color matrix, and M a combination of Y and Z bilinear spinor functions.

The Y functions are defined as

$$Y(p_1, \lambda_1; p_2, \lambda_2; c_R, c_L) = \bar{u}(p_1, \lambda_1)(c_R P_R + c_L P_L)u(p_2, \lambda_2). \tag{B.6}$$

Using (A.4), (A.5) and (A.9) and computing the resulting traces one easily finds

$$Y(p_1, +; p_2, +; c_R, c_L) = c_R \mu_1 \eta_2 + c_L \mu_2 \eta_1, \tag{B.7}$$

$$Y(p_1, +; p_2, -; c_R, c_L) = c_L S(+, p_1, p_2). \tag{B.8}$$

The remaining Y functions can be obtained by exchanging $+ \leftrightarrow -$ and $R \leftrightarrow L$.

For all processes we will only report those spinor functions M which are not related by a trivial relabeling of momenta and helicities. We also adopt the symbol $\{\lambda\}$ to denote a set of helicities of all external particles in a given reaction and $\Sigma_{\{\lambda\}}$ to indicate the usual sum over all possible helicity combinations. The expressions for the couplings c_R and c_L are given in table A.1. The amplitudes squared include the $1/n!$ factor for each n-uple of identical final-state particles. Therefore the phase-space integration must cover the whole space.

TABLE A.1
Right and left handed couplings of the fermions $f = \ell, q$ to the gauge bosons γ, Z, g. We have $(e^f, T_3^f, g^f) = (-1, -\frac{1}{2}, 0)$ for $f = e, \mu, \tau$; $(e^f, T_3^f, g^f) = (-\frac{1}{3}, -\frac{1}{2}, 1)$ for $f = d, s, b$ and $(e^f, T_3^f, g^f) = (\frac{2}{3}, \frac{1}{2}, 1)$ for $f = u, c$

Coupling	Gauge boson		
	γ	Z	g
c_R^f	e^f	$-e^f \sin^2\theta_W$	g^f
c_L^f	e^f	$T_3^f - e^f \sin^2\theta_W$	g^f

B.1. FOUR-FERMION PRODUCTION: $e^- e^+ \to f\bar{f} f' \bar{f}'$

The electroweak production of two leptons and two quarks and of four leptons ($\ell \neq e$),

$$e^-(p_1, \lambda_1) + e^+(p_2, \lambda_2) \to \ell^-(p_3, \lambda_3) + \ell^+(p_4, \lambda_4) + f(p_5, \lambda_5) + \bar{f}(p_6, \lambda_6), \tag{B.9}$$

is described in the case $f = \ell$ ($f \neq \ell$) by the eight (first four) Feynman diagrams of fig. B.1a plus the four (first two) of fig. B.1b. The matrix element is given by

$$|\overline{M}|^2_{\ell^-\ell^+ f\bar{f}} = \tfrac{1}{4} C^f \sum_{\{\lambda\}} \sum_{l,m=1}^{6} T_l^{\{\lambda\}} T_m^{\{\lambda\}*} \quad (f \neq \ell), \tag{B.10}$$

$$|\overline{M}|^2_{\ell^-\ell^+\ell^-\ell^+} = \tfrac{1}{16} C^f \sum_{\{\lambda\}} \sum_{l,m=1}^{12} T_l^{\{\lambda\}} T_m^{\{\lambda\}*}, \tag{B.11}$$

with the amplitudes

$$iT_k = e^4 \sum_{V=\gamma,Z} \sum_{V'=\gamma,Z} D_k \left(M_{k,VV'} - \frac{1}{M_Z^2} N_{k,VV'} \right), \quad k = 1, \ldots, 6(12), \tag{B.12}$$

where D_k denotes the propagator functions of the kth diagram.

In formula (B.12) the spinor functions $N_{k,VV'}$ corresponds to the $p^\mu p^\nu$ term of the Z propagator with momentum p, which is zero when acting on a massless fermion line. By definition $N_{k,V\gamma'} = 0$. For diagrams 5 through 8, 11 and 12 an additional minus sign has to be inserted because they are related to the remaining diagrams by the exchange of two identical fermions.

We have

$$M_{1,VV'} = \sum_{i=3,5,6} \sum_{\lambda=\pm} Z\left(p_5, \lambda_5; p_6, -\lambda_6; p_3, \lambda_3; p_i, \lambda; c^f_{R_{V'}}, c^f_{L_{V'}}; c^\ell_{R_V}, c^\ell_{L_{V'}}\right)$$
$$\times Z\left(p_i, \lambda; p_4, -\lambda_4; p_2, -\lambda_2; p_1, \lambda_1; c^\ell_{R_V}; c^e_{R_V}, c^\ell_{L_V}; c^e_{R_V}, c^e_{L_V}\right), \tag{B.13}$$

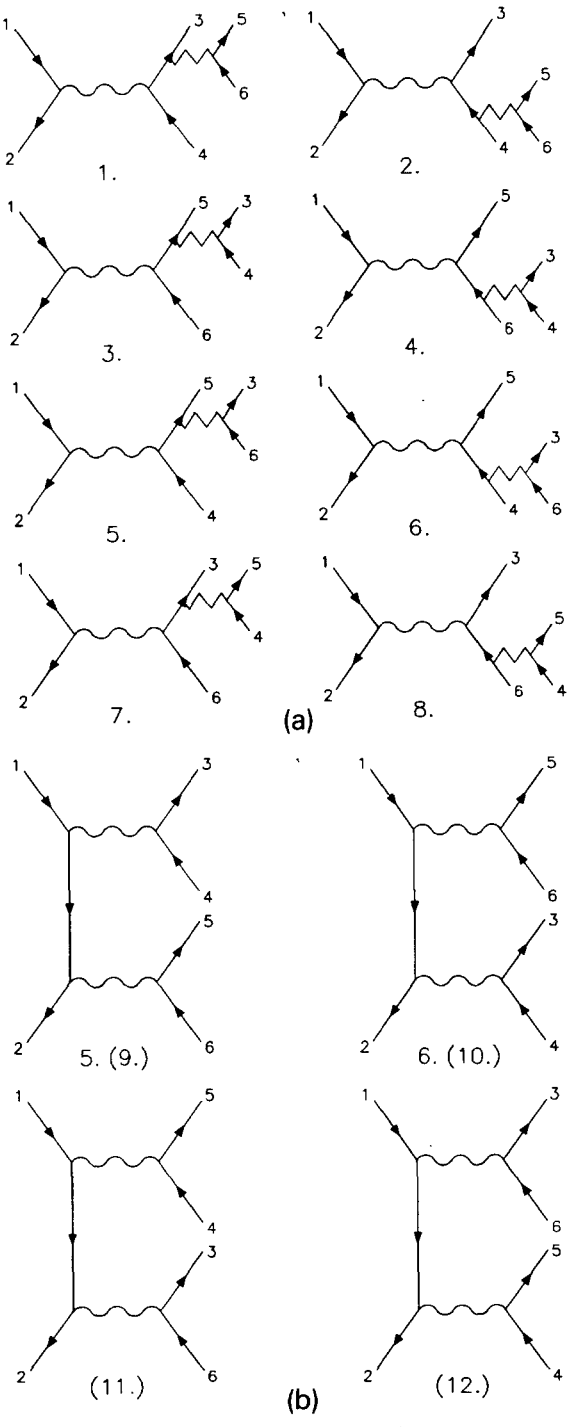

Fig. B.1. Feynman diagrams contributing in lowest order to $e^- e^+ \to q\bar{q}q'\bar{q}'$ (a) and to $e^- e^+ \to q\bar{q}\,\ell\bar{\ell}$ or $e^- e^+ \to \ell\bar{\ell}\ell'\bar{\ell}'$ (a and b) with ℓ, $\ell' \neq e$. If the two fermion pairs are not equal only the first four diagrams in (a) and the first two in (b) contribute. A wavy line represents a photon or a Z^0 while a jagged line represents a gluon, a photon or a Z^0. External lines are identified by their momentum as given in the text.

$$N_{1,VV'} = \sum_{i=3,5,6} \sum_{\lambda=\pm}$$

$$\left(\sum_{j=5,6} \sum_{\lambda'=\pm} Y(p_5, \lambda_5; p_j, \lambda'; 1, 1) Y\left(p_j, \lambda'; p_6, \lambda_6, c^{f}_{R_{V'}}, c^{f}_{L_{V'}}\right)\right)$$

$$\times \left(\sum_{k=5,6} \sum_{\lambda''=\pm} Y(p_3, \lambda_3; p_k, \lambda''; 1, 1) Y\left(p_k, \lambda''; p_i, \lambda; c^{\ell}_{R_{V'}}, c^{\ell}_{L_{V'}}\right)\right)$$

$$\times Z\left(p_i, \lambda; p_4, -\lambda_4; p_2, -\lambda_2; p_1, \lambda_1; c^{\ell}_{R_V}, c^{\ell}_{L_V}; c^{e}_{R_V}, c^{e}_{L_V}\right), \quad \text{(B.14)}$$

$$M_{2,VV'} = -\left[M_{1,VV'}(p_1 \leftrightarrow p_2, p_3 \leftrightarrow p_4, p_5 \leftrightarrow p_6;\right.$$

$$\left.\lambda_1 \leftrightarrow -\lambda_2, \lambda_3 \leftrightarrow -\lambda_4, \lambda_5 \leftrightarrow -\lambda_6)\right]^{*}, \quad \text{(B.15)}$$

$$N_{2,VV'} = -\left[N_{1,VV'}(p_1 \leftrightarrow p_2, p_3 \leftrightarrow p_4, p_5 \leftrightarrow p_6;\right.$$

$$\left.\lambda_1 \leftrightarrow -\lambda_2, \lambda_3 \leftrightarrow -\lambda_4, \lambda_5 \leftrightarrow -\lambda_6)\right]^{*}. \quad \text{(B.16)}$$

Then, the spinor functions corresponding to the diagrams of fig. B.1b are

$$M_{5(9),VV'} = -\sum_{i=1,3,4} b_i \sum_{\lambda=\pm}$$

$$Z\left(p_5, \lambda_5; p_6, -\lambda_6; p_2, -\lambda_2; p_i, \lambda; c^{f}_{R_{V'}}, c^{f}_{L_{V'}}; c^{e}_{R_{V'}}, c^{e}_{L_{V'}}\right)$$

$$\times Z\left(p_3, \lambda_3; p_4, -\lambda_4; p_i, \lambda; p_1, \lambda_1; c^{\ell}_{R_V}, c^{\ell}_{L_V}; c^{e}_{R_V}, c^{e}_{L_V}\right), \quad \text{(B.17)}$$

where

$$b_1 = -b_3 = -b_4 = -b_5 = -b_6 = -1. \quad \text{(B.18)}$$

Notice that

$$N_{k+4(k+8),VV'} = 0, \quad k = 1, 2(1, \ldots, 4), \quad \text{(B.19)}$$

since the Z propagators are always connected to a massless electron line. Finally, in formulae (B.10), (B.11) C^{f} indicates the color factor

$$C^{\ell} = 1 \quad \text{or} \quad C^{q} = 3. \quad \text{(B.20)}$$

The three-level Feynman diagrams describing the reaction

$$e^{-}(p_1, \lambda_1) + e^{+}(p_2, \lambda_2)$$

$$\rightarrow q(p_3, \lambda_3) + \bar{q}(p_4, \lambda_4) + q'(p_5, \lambda_5) + \bar{q}'(p_6, \lambda_6) \quad \text{(B.21)}$$

are shown in fig. B.1a (Only the first four contribute if $q \neq q'$). The general form of the amplitude squared is

$$|\overline{M}|^2_{q\bar{q}q'\bar{q}'} = \tfrac{1}{4}\sum_{\{\lambda\}}\sum_{l,m=1}^{4} T_l^{\{\lambda\}} T_m^{\{\lambda\}*} C_{lm} \quad (q \neq q'), \tag{B.22}$$

$$|\overline{M}|^2_{q\bar{q}q\bar{q}} = \tfrac{1}{16}\sum_{\{\lambda\}}\sum_{l,m=1}^{8} T_l^{\{\lambda\}} T_m^{\{\lambda\}*} C_{lm}, \tag{B.23}$$

where C is an 8×8 matrix containing the color factors, and

$$iT_k = g_s^2 e^2 \sum_{V=\gamma,Z} D_k M_{k,V}, \quad k = 1,\ldots,4(8), \tag{B.24}$$

are the individual amplitudes.

The spinor functions and the propagators can be obtained from the corresponding expressions for the case $e^-e^+ \to \ell\bar{\ell}f\bar{f}$ identifying $V' \to g$, $\ell \to q$ and $f \to q'$.

Finally, the matrix of the color factors is

$$C = \begin{pmatrix} \alpha & \alpha & \alpha & \alpha & \beta & \beta & \beta & \beta \\ \alpha & \alpha & \alpha & \alpha & \beta & \beta & \beta & \beta \\ \alpha & \alpha & \alpha & \alpha & \beta & \beta & \beta & \beta \\ \alpha & \alpha & \alpha & \alpha & \beta & \beta & \beta & \beta \\ \beta & \beta & \beta & \beta & \alpha & \alpha & \alpha & \alpha \\ \beta & \beta & \beta & \beta & \alpha & \alpha & \alpha & \alpha \\ \beta & \beta & \beta & \beta & \alpha & \alpha & \alpha & \alpha \\ \beta & \beta & \beta & \beta & \alpha & \alpha & \alpha & \alpha \end{pmatrix}, \quad \alpha = 2, \quad \beta = -\tfrac{2}{3}. \tag{B.25}$$

B.2. TWO-FERMION AND ONE-BOSON PRODUCTION: $e^-e^+ \to f\bar{f}V$

For Z, γ production in association with an $f\bar{f}$ pair ($f \neq e$) in

$$e^-(p_1, \lambda_1) + e^+(p_2, \lambda_2) \to f(p_3, \lambda_3) + \bar{f}(p_4, \lambda_4) + Z, \gamma(p_5, \lambda_5) \tag{B.26}$$

the Feynman graphs are depicted in figs. B.2a and B.2b. For γ production the amplitude squared is

$$|\overline{M}|^2_{f\bar{f}\gamma} = \tfrac{1}{4}C^f \sum_{\{\lambda\}}\sum_{l,m=1}^{4} T_l^{\{\lambda\}} T_m^{\{\lambda\}*}, \tag{B.27}$$

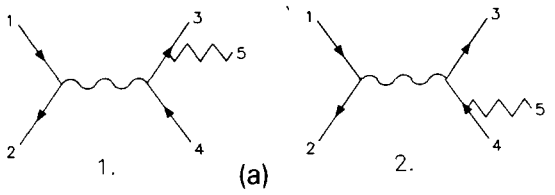

Fig. B.2. Feynman diagrams contributing in lowest order to $e^-e^+ \to q\bar{q}g$ (a) and to $e^-e^+ \to q\bar{q}V$, $V = \gamma, Z$ (a and b). A wavy line represents a photon or a Z^0 while a jagged line represents a gluon, a photon or a Z^0. External lines are identified by their momentum as given in the text.

where

$$-iT_k = e^3 \sum_{V=\gamma,Z} D_k M_{k,V}, \quad k = 1, \ldots, 4. \tag{B.28}$$

Recalling that q_i is the auxiliary quadrimomentum of the polarization vector corresponding to the massless boson of momentum p_i, the $M_{k,V}$ functions are

$$M_{1,V} = N_5 \sum_{i=3,5} \sum_{\lambda=\pm} Z\left(p_5, \lambda_5; q_5, \lambda_5; p_3, \lambda_3; p_i, \lambda; 1, 1; c^f_{R_\gamma}, c^f_{L_\gamma}\right)$$

$$\times Z\left(p_i, \lambda; p_4, -\lambda_4; p_2, -\lambda_2; p_1, \lambda_1; c^f_{R_V}, c^f_{L_V}; c^e_{R_V}, c^e_{L_V}\right), \tag{B.29}$$

$$M_{2,V} = -\left[M_{1,V}(p_1 \leftrightarrow p_2, p_3 \leftrightarrow p_4, p_5 \leftrightarrow q_5; \lambda_1 \leftrightarrow -\lambda_2, \lambda_3 \leftrightarrow -\lambda_4)\right]^*, \tag{B.30}$$

$$M_{3,V} = N_5 \sum_{i=2,5} b_i \sum_{\lambda=\pm} Z\left(p_3, \lambda_3; p_4, -\lambda_4; p_i, \lambda; p_1, \lambda_1; c^f_{R_V}, c^f_{L_V}; c^e_{R_V}, c^e_{L_V}\right)$$

$$\times Z\left(p_5, \lambda_5; q_5, \lambda_5; p_2, -\lambda_2; p_i, \lambda; 1, 1; c^e_{R_\gamma}, c^e_{L_\gamma}\right), \tag{B.31}$$

$$M_{4,V} = -\left[M_{3,V}(p_1 \leftrightarrow p_2, p_3 \leftrightarrow p_4, p_5 \leftrightarrow q_5; \lambda_1 \leftrightarrow -\lambda_2, \lambda_3 \leftrightarrow -\lambda_4; b_1 \leftrightarrow b_2)\right]^*. \tag{B.32}$$

For Z production the amplitude squared has the form

$$|\overline{M}|^2_{f\bar{f}Z} = \tfrac{1}{4} C^f \sum_{\{\lambda\}} \frac{3}{8\pi m_Z^2} \int d\Omega \sum_{l,m=1}^{4} T_l^{\{\lambda\}} T_m^{\{\lambda\}*}, \tag{B.33}$$

where

$$-iT_k = \frac{e^3}{\sin\theta_W \cos\theta_W} \sum_{V=\gamma,Z} D_k M_{k,V}, \quad k = 1, \ldots, 4. \tag{B.34}$$

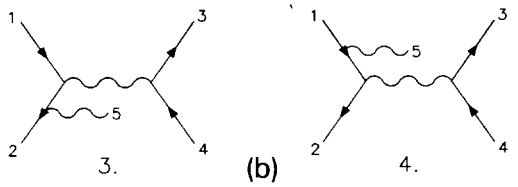

Fig. B.2 (continued).

The $M_{k,\mathrm{V}}$ functions can be obtained from eqs. (B.29) through (B.32) with the following substitutions: $p_5 \to r_1$, $q_5 \to r_2$, $\lambda_5 \to -$, $N_5 \to 1$, $c_{\mathrm{L}\gamma}^{\mathrm{e,f}} \to c_{\mathrm{L}Z}^{\mathrm{e,f}}$ and $c_{\mathrm{R}\gamma}^{\mathrm{e,f}} \to c_{\mathrm{R}Z}^{\mathrm{e,f}}$, where r_1 and r_2 are the auxiliary momenta of the polarization vector for the Z.

The color factor is

$$C^{\ell} = 1 \quad \text{or} \quad C^{q} = 3. \tag{B.35}$$

The Feynman graphs for

$$\mathrm{e}^-(p_1, \lambda_1) + \mathrm{e}^+(p_2, \lambda_2) \to \mathrm{q}(p_3, \lambda_3) + \bar{\mathrm{q}}(p_4, \lambda_4) + \mathrm{g}(p_5, \lambda_5) \tag{B.36}$$

are depicted in fig. B.2a. The amplitude squared is

$$|\overline{M}|^2_{\mathrm{q\bar{q}g}} = \tfrac{1}{4} C \sum_{\{\lambda\}} \sum_{l,m=1}^{2} T_l^{\{\lambda\}} T_m^{\{\lambda\}*}, \tag{B.37}$$

where

$$-iT_k = g_{\mathrm{s}} e^2 \sum_{\mathrm{V}=\gamma,\mathrm{Z}} D_k M_{k,\mathrm{V}}, \quad k = 1, 2. \tag{B.38}$$

The spinor functions can be obtained from the corresponding expressions for $\mathrm{e}^-\mathrm{e}^+ \to \mathrm{q\bar{q}}\gamma$ substituting $c_{\mathrm{R}\gamma}^{\mathrm{q}}$, $c_{\mathrm{L}\gamma}^{\mathrm{q}}$ with $c_{\mathrm{Rg}}^{\mathrm{q}}$, $c_{\mathrm{Lg}}^{\mathrm{q}}$.

The color factor is

$$C = 4. \tag{B.39}$$

B.3. TWO-FERMION AND TWO-BOSON PRODUCTION: $\mathrm{e}^-\mathrm{e}^+ \to \mathrm{f\bar{f}VV'}$

The Feynman diagrams corresponding to

$$\begin{aligned} &\mathrm{e}^-(p_1, \lambda_1) + \mathrm{e}^+(p_2, \lambda_2) \\ &\quad \to \mathrm{q}(p_3, \lambda_3) + \bar{\mathrm{q}}(p_4, \lambda_4) + \mathrm{g}(p_5, \lambda_5) + \mathrm{g}(p_6, \lambda_6) \end{aligned} \tag{B.40}$$

are shown in figs. B.3a and B.3b. The amplitude squared for this process is

$$|\overline{M}|^2_{\mathrm{q\bar{q}gg}} = \tfrac{1}{8} \sum_{\{\lambda\}} \sum_{l,m=1}^{8} T_l^{\{\lambda\}} T_m^{\{\lambda\}*} C_{lm}, \tag{B.41}$$

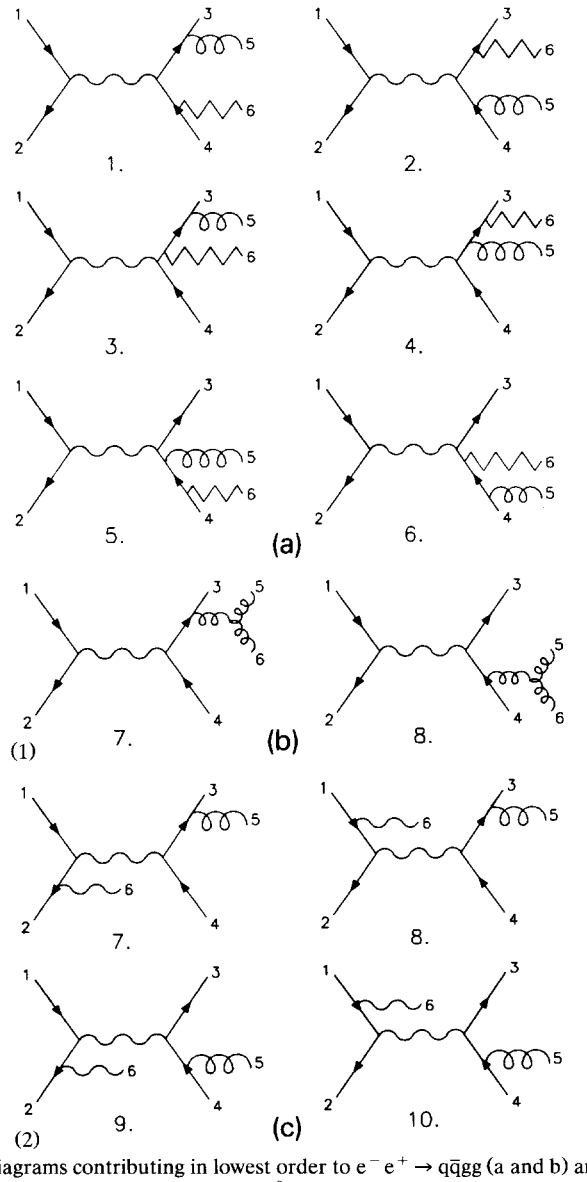

Fig. B.3. Feynman diagrams contributing in lowest order to $e^- e^+ \to q\bar{q}gg$ (a and b) and to $e^- e^+ \to q\bar{q}g\gamma$ (a and c). A wavy line represents a photon or a Z^0 while a jagged line represents a gluon or a photon. External lines are identified by their momentum as given in the text.

with the amplitudes

$$-iT_k = g_s^2 e^2 \sum_{V=\gamma,Z} D_k M_{k,V}, \quad k = 1,\ldots,8. \tag{B.42}$$

Recalling that q_i is the auxiliary quadrimomentum of the polarization vector

corresponding to the massless boson of momentum p_i, one gets for the spinor functions:

$$M_{1,V} = N_5 N_6 \sum_{i=3,5} \sum_{j=4,6} \sum_{\lambda=\pm} \sum_{\lambda'=\pm}$$

$$Z(p_5, \lambda_5; q_5, \lambda_5; p_3, \lambda_3; p_i, \lambda; 1, 1; c^q_{R_g}, c^q_{L_g})$$

$$\times Z(p_i, \lambda; p_j, \lambda'; p_2, -\lambda_2; p_1, \lambda_1; c^q_{R_V}, c^q_{L_V}; c^e_{R_V}, c^e_{L_V})$$

$$\times Z(p_6, \lambda_6; q_6, \lambda_6; p_j, \lambda'; p_4, -\lambda_4; 1, 1; c^q_{R_g}, c^q_{L_g}), \tag{B.43}$$

$$M_{3,V} = N_5 N_6 \sum_{i=3,5} \sum_{j=3,5,6} \sum_{\lambda=\pm} \sum_{\lambda'=\pm}$$

$$Z(p_5, \lambda_5; q_5, \lambda_5; p_3, \lambda_3; p_i, \lambda; 1, 1; c^q_{R_g}, c^q_{L_g})$$

$$\times Z(p_6, \lambda_6; q_6, \lambda_6; p_i, \lambda; p_j, \lambda'; 1, 1; c^q_{R_g}, c^q_{L_g})$$

$$\times Z(p_j, \lambda'; p_4, -\lambda_4; p_2, -\lambda_2; p_1, \lambda_1; c^q_{R_V}, c^q_{L_V}; c^e_{R_V}, c^e_{L_V}), \tag{B.44}$$

$$M_{5,V} = [M_{3,V}(p_1 \leftrightarrow p_2, p_3 \leftrightarrow p_4, p_5 \leftrightarrow q_6, q_5 \leftrightarrow p_6;$$

$$\lambda_1 \leftrightarrow -\lambda_2, \lambda_3 \leftrightarrow -\lambda_4, \lambda_5 \leftrightarrow \lambda_6)]^*, \tag{B.45}$$

$$M_{7,V} = N_5 N_6 \sum_{i=3,5,6} \sum_{\lambda=\pm} \sum_{\lambda'=\pm}$$

$$\{2Z(p_3, \lambda_3; p_i, \lambda; p_5, \lambda_5; q_5, \lambda_5; c^q_{R_g}, c^q_{L_g}; 1, 1)$$

$$\times Y(p_6, \lambda_6; p_5, \lambda'; 1, 1) Y(p_5, \lambda'; q_6, \lambda_6; 1, 1)$$

$$+ Z(p_5, \lambda_5; q_5, \lambda_5; p_6, \lambda_6; q_6, \lambda_6; 1, 1; 1, 1)$$

$$\times [Y(p_3, \lambda_3; p_6, \lambda'; 1, 1) Y(p_6, \lambda'; p_i, \lambda; 1, 1)$$

$$- Y(p_3, \lambda_3; p_5, \lambda'; 1, 1) Y(p_5, \lambda'; p_i, \lambda; 1, 1)]$$

$$- 2Z(p_6, \lambda_6; q_6, \lambda_6; p_3, \lambda_3; p_i, \lambda; 1, 1; c^q_{R_g}, c^q_{L_g})$$

$$\times Y(p_5, \lambda_5; p_6, \lambda'; 1, 1) Y(p_6, \lambda'; q_5, \lambda_5; 1, 1)\}$$

$$\times Z(p_i, \lambda; p_4, -\lambda_4; p_2, -\lambda_2; p_1, \lambda_1; c^q_{R_V}, c^q_{L_V}; c^e_{R_V}, c^e_{L_V}), \tag{B.46}$$

$$M_{8,V} = -[M_{7,V}(p_1 \leftrightarrow p_2, p_3 \leftrightarrow p_4; \lambda_1 \leftrightarrow -\lambda_2, \lambda_3 \leftrightarrow -\lambda_4)]^* \tag{B.47}$$

In this case, the matrix of the color factors is

$$C = \begin{pmatrix} \gamma & \delta & \gamma & \delta & \gamma & \delta & \epsilon & \epsilon \\ \delta & \gamma & \delta & \gamma & \delta & \gamma & -\epsilon & -\epsilon \\ \gamma & \delta & \gamma & \delta & \gamma & \delta & \epsilon & \epsilon \\ \delta & \gamma & \delta & \gamma & \delta & \gamma & -\epsilon & -\epsilon \\ \gamma & \delta & \gamma & \delta & \gamma & \delta & \epsilon & \epsilon \\ \delta & \gamma & \delta & \gamma & \delta & \gamma & -\epsilon & -\epsilon \\ \epsilon & -\epsilon & \epsilon & -\epsilon & \epsilon & -\epsilon & \zeta & \zeta \\ \epsilon & -\epsilon & \epsilon & -\epsilon & \epsilon & -\epsilon & \zeta & \zeta \end{pmatrix},$$

$$\gamma = \tfrac{16}{3}, \quad \delta = -\tfrac{2}{3}, \quad \epsilon = 6, \quad \zeta = 12. \tag{B.48}$$

The Feynman diagrams corresponding to the process

$$\begin{aligned} &e^-(p_1, \lambda_1) + e^+(p_2, \lambda_2) \\ &\quad \to q(p_3, \lambda_3) + \bar{q}(p_4, \lambda_4) + g(p_5, \lambda_5) + \gamma(p_6, \lambda_6) \end{aligned} \tag{B.49}$$

are depicted in fig. B.3a and B.3c. The amplitude squared is

$$|\overline{M}|^2_{q\bar{q}g\gamma} = \tfrac{1}{4} C \sum_{\{\lambda\}} \sum_{l,m=1}^{10} T_l^{\{\lambda\}} T_m^{\{\lambda\}*}, \tag{B.50}$$

with the amplitudes

$$-iT_k = \sum_{V=\gamma,Z} g_s e^3 D_k M_{k,V}, \quad k = 1, \ldots, 10. \tag{B.51}$$

The spinor functions $M_{1,V}$ through $M_{6,V}$ can be obtained from the corresponding expressions for $e^-e^+ \to q\bar{q}gg$ substituting $c^q_{R_g}$, $c^q_{L_g}$ with $c^q_{R_\gamma}$, $c^q_{L_\gamma}$ in the Z functions which have both p_6 and q_6 as arguments.

The remaining spinor functions are

$$\begin{aligned} M_{7,V} = N_5 N_6 &\sum_{i=3,5} \sum_{j=2,6} b_j \sum_{\lambda=\pm} \sum_{\lambda'=\pm} \\ &Z(p_5, \lambda_5; q_5, \lambda_5; p_3, \lambda_3; p_i, \lambda; 1, 1; c^q_{R_g}, c^q_{L_g}) \\ &\times Z(p_i, \lambda; p_4, -\lambda_4; p_j, \lambda'; p_1, \lambda_1; c^q_{R_V}, c^q_{L_V}; c^e_{R_V}, c^e_{L_V}) \\ &\times Z(p_6, \lambda_6; q_6, \lambda_6; p_2, -\lambda_2; p_j, \lambda'; 1, 1; c^e_{R_\gamma}, c^e_{L_\gamma}), \end{aligned} \tag{B.52}$$

$$M_{8,V} = -N_5 N_6 \sum_{i=3,5} \sum_{j=1,6} b_j \sum_{\lambda=\pm} \sum_{\lambda'=\pm}$$

$$Z\left(p_5, \lambda_5; q_5, \lambda_5; p_3, \lambda_3; p_i, \lambda; 1, 1; c^q_{R_g}, c^q_{L_g}\right)$$

$$\times Z\left(p_i, \lambda; p_4, -\lambda_4; p_2, -\lambda_2; p_j, \lambda'; c^q_{R_V}, c^q_{L_V}; c^e_{R_V}, c^e_{L_V}\right)$$

$$\times Z\left(p_6, \lambda_6; q_6, \lambda_6; p_j, \lambda'; p_1, \lambda_1; 1, 1; c^e_{R_\gamma}, c^e_{L_\gamma}\right), \tag{B.53}$$

$$M_{9,V} = \left[M_{8,V}(p_1 \leftrightarrow p_2, p_3 \leftrightarrow p_4; \lambda_1 \leftrightarrow -\lambda_2, \lambda_3 \leftrightarrow -\lambda_4; b_1 \leftrightarrow b_2)\right]^*, \tag{B.54}$$

$$M_{10,V} = \left[M_{7,V}(p_1 \leftrightarrow p_2, p_3 \leftrightarrow p_4; \lambda_1 \leftrightarrow -\lambda_2, \lambda_3 \leftrightarrow -\lambda_4; b_1 \leftrightarrow b_2)\right]^*, \tag{B.55}$$

where

$$b_1 = b_2 = -b_6 = -1. \tag{B.56}$$

Finally, the color factor is

$$C = 4. \tag{B.57}$$

References

[1] A. Ballestrero, E. Maina and S. Moretti, Phys. Lett. B294 (1992) 425
[2] S.L. Wu et al., *in* Proc. ECFA Workshop on LEP 200, Aachen, Germany, 1986, CERN 87-08, eds. A. Bohm and W. Hoogland
[3] B.L. Ioffe, Phys. Lett. B78 (1978) 277
[4] G. Branco, K.H. Streng and H.P. Nilles, Phys. Lett. B85 (1979) 269
[5] A. Ali et al., Nucl. Phys. B167 (1980) 454;
J. Körner et al., Nucl. Phys. B185 (1981) 365
[6] K.J.F. Gaemers and J.A.M. Vermaseren, Z. Phys. C7 (1980) 81
[7] R.K. Ellis, D.A. Ross and A.E. Terrano, Nucl. Phys. B178 (1981) 421
[8] O. Nachtmann and A. Reiter, Z. Phys. C16 (1982) 45
[9] D. Danckaert et al., Phys. Lett. B114 (1982) 203
[10] L. Clavelli and G.V. Gehlen, Phys. Rev. D27 (1983) 1495
[11] F.A. Berends, P.H. Daverveldt and R. Kleiss, Phys. Lett. B148 (1984) 489; Nucl. Phys. B253 (1985) 441
[12] E. Laermann, K.H. Streng and P.M. Zerwas, Z. Phys. C3 (1980) 289
[13] J. Jersák, E. Laermann and P.M. Zerwas, Phys. Rev. D25 (1982) 1218
[14] E.W.N. Glover, R. Kleiss and J.J. van der Bij, Z. Phys. C47 (1990) 435
[15] E.N. Argyres, C.G. Papadopoulos and S.D.P. Vlassopulos, Phys. Lett. B237 (1990) 581
[16] G. Altarelli and B. Lampe, Nucl. Phys. B391 (1993) 3
[17] M.L. Mangano and S.J. Parke, Phys. Rep. 200 (1991) 301
[18] C. Mana and M. Martinez, Nucl. Phys. B287 (1987) 601
[19] R. Kleiss and W.J. Stirling, Nucl. Phys. B262 (1985) 235
[20] K. Hagiwara and D. Zeppenfeld, Nucl. Phys. B274 (1986) 1
[21] G.J. Gounaris, R. Kogerler and H. Neufeld, Phys. Rev. D34 (1986) 3257

[22] L3 Collaboration, B. Adeva et al., Phys. Lett. B248 (1990) 464;
OPAL Collaboration, M.Z. Akrawy et al., Phys. Lett. B235 (1990) 389;
OPAL Collaboration, M.Z. Akrawy et al., Z. Phys. C49 (1991) 375;
ALEPH Collaboration, D. Decamp et al., Phys. Lett. B255 (1991) 623;
DELPHI Collaboration, P. Abreu et al., Phys. Lett. B247 (1990) 167;
MARK II Collaboration, S. Komamiya et al., Phys. Rev. Lett. 64 (1990) 987;
DELPHI Collaboration, P. Abreu et al., Z. Phys. C54 (1992) 55;
ALEPH Collaboration, D. Decamp et al., Phys. Lett. B284 (1992) 163;
OPAL Collaboration, P.D. Acton et al., Z. Phys. C55 (1992) 1;
L3 Collaboration, B. Adeva et al., Z. Phys. C55 (1992) 39;
ALEPH Collaboration, D. Buskulic et al., Z. Phys. C55 (1992) 209;
OPAL Collaboration, P.D. Acton et al., preprint CERN-PPE/93-38
[23] L3 Collaboration, B. Adeva et al., Phys. Lett. B271 (1991) 461;
DELPHI Collaboration, P. Abreu et al., preprint CERN-PPE/93-59
[24] L3 Collaboration, B. Adeva et al., Phys. Lett. B263 (1991) 551;
DELPHI Collaboration, P. Abreu et al., Phys. Lett. B274 (1992) 498;
OPAL Collaboration, G. Alexander et al., Z. Phys. C52 (1991) 543
[25] L3 Collaboration, B. Adeva et al., Phys. Lett. B248 (1990) 227;
OPAL Collaboration, M.Z. Akrawy et al., Z. Phys. C49 (1991) 49
[26] DELPHI Collaboration, P. Abreu et al., Phys. Lett. B255 (1991) 466;
ALEPH Collaboration, D. Decamp et al., Phys. Lett. B284 (1992) 151
[27] OPAL Collaboration, G. Alexander et al., Phys. Lett. B265 (1991) 462
[28] JADE Collaboration, W. Bartel et al., Z. Phys. C33 (1986) 23;
JADE Collaboration, S. Bethke et al., Phys. Lett. B213 (1988) 235
[29] N. Brown and W.J. Stirling, Phys. Lett. B252 (1990) 657; Z. Phys. C53 (1992) 629
[30] Z. Kunszt and P. Nason, *in* Z Physics at LEP I, eds. G. Altarelli, R Kleiss and C. Verzegnassi, CERN 89-08 (1989)
[31] ALEPH Collaboration, D. Decamp et al., Phys. Lett. B263 (1991) 112
[32] OPAL Collaboration, P.D. Acton et al., preprint CERN-PPE-92-57 (April 1992)
[33] J. Hilgart, R. Kleiss and F. Le Diberder, preprint CERN-PPE-92-115 (July 1992)
[34] G.P. Lepage, J. Comp. Phys. 27 (1978) 192
[35] S. Cartwright, ed., Proc. Workshop on Photon radiation from quarks, Annecy, France, 1991, CERN 92-04
[36] OPAL Collaboration, G. Alexander et al., Phys. Lett. B264 (1991) 219;
OPAL Collaboration, P.D. Acton et al., Z. Phys. C54 (1992) 193;
ALEPH Collaboration, D. Decamp et al., Phys. Lett. B264 (1991) 476;
DELPHI Collaboration, P. Abreu et al., Z. Phys. C53 (1992) 555;
L3 Collaboration, O. Adriani et al., Phys. Lett. B292 (1992) 472
[37] T. Sjöstrand, Comp. Phys. Comm. 39 (1986) 347; 43 (1987) 367;
M. Bengtsson and T. Sjöstrand, Nucl. Phys. B289 (1987) 810